Nuclear structure effects in preequilibrium reactions: α-induced reactions on ^{24,25,26}Mg, ^{27}Al, and ^{28}Si

H. Machner, G. Seniwongse, P. Jahn, M. Nolte, M. Rogge, and P. Turek
Institut für Kernphysik, Kernforschungsanlage Jülich, D-5170 Jülich, Federal Republic of Germany
(Received 24 December 1985)

We have measured charged particle spectra from 100 MeV α-induced reactions on targets of ^{24,25,26}Mg, ^{27}Al, and ^{28}Si. The charged particles are protons, deuterons, tritons, ^{3}He, and α particles. The cross sections were analyzed in the framework of the exciton coalescence model. The data suggest complex particle formation to be independent of individual nuclear structure. The deduced single-particle state densities show strong odd-even effects.

I. INTRODUCTION

The study of continuous particle spectra is of great interest because the corresponding yield exhausts the largest fraction of the absorption cross section. Systematic experimental studies performed so far have investigated reactions on target nuclei spanning the periodic table.[1-6] From these measurements bulk properties of the underlying reaction mechanism have been learned. Typical information, for instance, is the A dependence of the inelastic cross section which is $(200\pm10)A^{1/3}$ (mb) for (p,p') reactions at $E_p=90$ MeV.[3] This dependence suggests the surface dominance of the reaction. Investigations, concerning the question whether and, if yes, to what extent the individual nuclear structure influences the continuous spectra, are scarce. Castaneda *et al.*[7] have studied (n,p) reactions on all even-even Ni isotopes. They concluded from their data analysis that spectral height differences are due to neutron skins with different thicknesses. The Livermore-Hamburg group has studied single-particle effects by investigating the high energy part of the neutron spectra from 25 MeV (p,n) reactions especially on nuclei below the $f_{7/2}$ shell closure and above the $g_{9/2}$ shell closure.[8-10]

In the present investigation we have studied nuclear reactions induced by a 100 MeV α-particle beam on targets of ^{24,25,26}Mg, ^{27}Al, and ^{28}Si. Another region in the periodic table containing a large number of neighboring stable isotopes suited as nuclear targets is around $A\sim115$. Most of them are Sn isotopes having the magic proton number $Z=50$. In the present study light nuclei were the preferable choice, because light nuclei have less dense spaced levels than heavy ones. There is hope, therefore, that one can see influences of nuclear structure on secondary particle spectra more clearly than would be the case for heavy nuclei. Furthermore, this list of targets contains even-even as well as even-odd and odd-even nuclei. Moreover, the nuclei ^{24}Mg and ^{28}Si are so-called "α-substructure" nuclei because one can think of them as being made up of 6 and 7 α particles, respectively.

If this substructure played an important role one would expect an increase in the (α,α') yields due to knockout contributions in cases of the two "α nuclei" with respect to the other target nuclei.

The paper is arranged as follows. In the next section details of the experiments are given. In Sec. III we discuss the experimental findings. Then the data are compared against model predictions and our conclusions follow.

II. EXPERIMENTS

The experiments were carried out at the Jülich isochronous cyclotron JULIC. The α beam was focused with the aid of a pair of quadrupole magnets to the center of a scattering chamber 1 m in diameter. The beam was then refocused by another magnetic quadrupole lens to an external Faraday cup also serving as beam dump. The targets used—except the Si target—were metallic self-supporting foils made from isotopically enriched (Mg) or isotopically pure materials. They where produced by rolling and their thicknesses are given in Table I. The Si target was fabricated from a very pure Si crystal (99.9% purity) of natural isotopic distribution by grinding. This

TABLE I. Properties of the targets used in the experiments.

Target	Isotopic abundance (%)	Thickness (mg/cm^2)
^{24}Mg	99.9	9.95 self-supporting foil
^{25}Mg	99.2	5.6 self-supporting foil
^{26}Mg	99.4	5.29 self-supporting foil
^{27}Al	100	5.2 self-supporting foil
^{28}Si	92.2	5.99 on Mylar backing

crystal was then glued onto a Mylar foil as backing.

The secondary charged particles were detected with two solid-state detector telescopes mounted 3° apart from each other on the revolving top of the scattering chamber. Both consist of Ge(Li)-E detectors with thicknesses sufficient to stop 100 MeV protons. One telescope was tailored to detect hydrogen isotopes and the other to detect helium isotopes. Therefore, the ΔE detectors of the telescopes were a 1000 μm Si surface-barrier detector and a 400 μm Si surface-barrier detector, respectively. The solid angles, defined by 5 mm thick tantalum apertures, were 8.55×10^{-5} sr and 1.28×10^{-4} sr and the angle openings 0.958 and 0.731 deg for the "hydrogen telescope" and the "helium telescope," respectively.

Particle identification was performed by feeding the analog ΔE and $(\Delta E+E)$ signals into analog-to-digital converters (ADC's) of the on-line data acquisition system ND6660 and employing its on-line sorting possibilities. In this method two-dimensional curved gates had to be set around the event islands corresponding to different ejectiles on a ΔE-$(\Delta E+E)$ map. Particle analyzed energy spectra were recorded on magnetic tape after the end of each run. The setting of the gates was controlled on the screen of the ND6660. Because of the limited channel resolution of this display, data were taken from time to time on tape in the list mode and plotted on a high resolution screen together with the gates to control their setting. The dead time of the electronic setup and the data acquisition system were measured by feeding signals into the preamplifiers from a pulse generator which was triggered by the down-scaled counting rate of the "helium telescope." The dead time was 0.5% to 7% depending on the counting rate. The measured beam charge was corrected correspondingly.

The telescopes were energy calibrated by detecting inelastic scattered α particles on ^{12}C and protons, deuterons, and α particles from elastic scattering processes on $(CH_2)_x$-$(CD_2)_x$ targets. This procedure yielded a linear relationship between energy and ADC-channel number. Finally, the counting rate was converted into cross sections. The systematic errors were estimated to be 10% in solid angle and 2% in the measured charge. The inhomogenities in the targets were up to 5% and their total thickness uncertainty 1%. Since the beam spot of 3 mm in diameter averages over a part of the target area, an uncertainty of 3% was assumed. The cross sections were averaged over 2 MeV wide bins, thus reducing counting rate errors. The total cross sections estimated were thus incorrect by typically 4.4% at an angle of 30°. The cross sections and deduced angle integrated yields are tabulated in Ref. 11.

III. EXPERIMENTAL RESULTS

The measured spectra show a large continuous part with rather remarkable differences in shape for the different particle types being emitted. This is especially visible at forward angles. In Fig. 1 charged particle spectra from particles emerging from the ^{28}Si plus α-particle system at $\vartheta=12°$ are shown. All spectra except the proton spectrum show at the high energy end lines due to nuclear

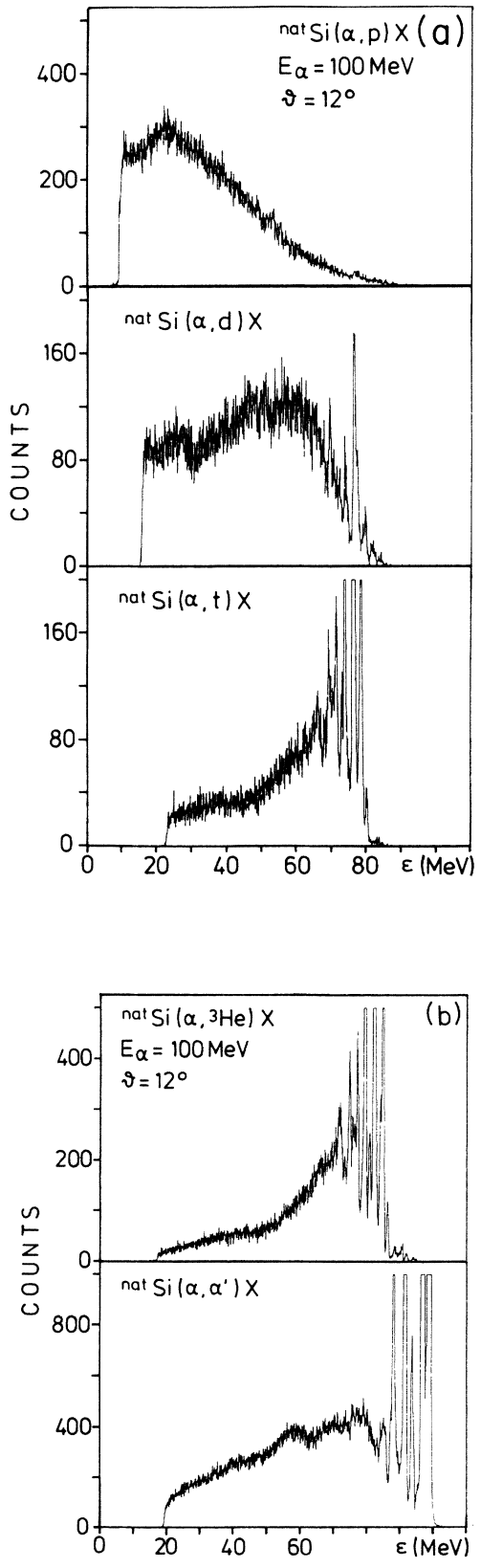

FIG. 1. (a) Hydrogen isotope spectra from the α plus ^{28}Si interactions. Data are taken at $\vartheta=12°$. (b) Same as (a) but for helium isotopes.

reactions to excited bound states in the corresponding residual system. This structure is especially rich for inelastic scattering and one particle transfer reactions. Two particle transfer seems to be less probable and obviously there is no three particle transfer visible, at least on the level of the present statistics. All spectra show bell-shaped bumps in the continuous part. For particles lighter than α particles they are centered around the beam velocity and are due to breakup of the projectile α particle.[12,13] The ratio between the yield contained in the bumps and in the underlying "background" increases with increasing particle mass number: $\sim$0.36, 0.41, 1, and 1 for p, d, t, and ^{3}He. In the d spectra a second but much smaller structure when compared to the breakup is visible but at approximately half the beam velocity. It may correspond to a breakup reaction followed by neutron pickup: (α,p)(p,d). A similar process has been reported for the case of the (^{3}He,t) reaction:[5] (^{3}He,d)(d,t). The question whether other reactions of this type are present like (α,d)(d,t) cannot be answered with the present data because of the statistics and too large detection angles. The same is true for the process (α,^{3}He)(^{3}He,α'), because in the inelastic α spectra contributions from the reversed process, i.e., pickup followed by breakup[14] due to particle unstable intermediate systems ^{5}He or ^{5}Li are present. However, for larger angles these contributions to the cross sections stemming mainly from the projectile are small and not even visible in the angle integrated data. The data are similar in their behavior with respect to angular distributions or shapes as previous ones from 140 MeV incident α particles.[3] We will therefore concentrate on specific results of the present data. In Fig. 2 the angle-integrated cross sections for (α,p) reactions on the different target nuclei are shown. Surprisingly, the lightest target nucleus under consideration in the present investigation, namely ^{24}Mg, yields the largest cross section followed by the one for ^{28}Si which is also an "α nucleus." The cross sections for ^{25}Mg and

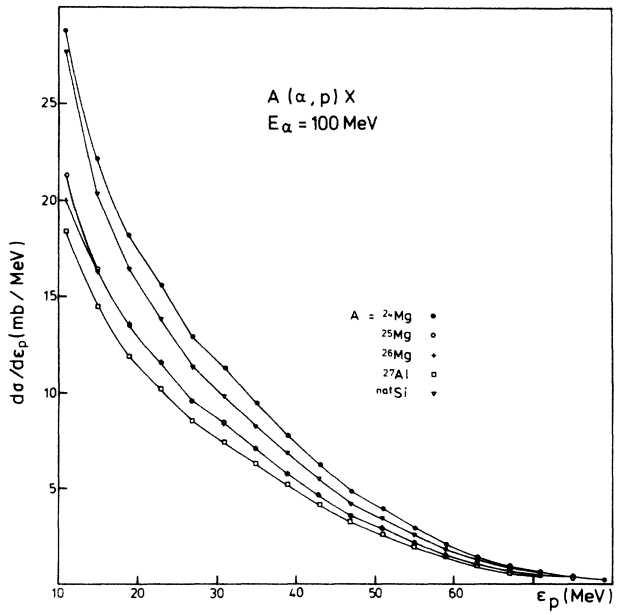

FIG. 2. Angle integrated cross sections for (α,p) reactions.

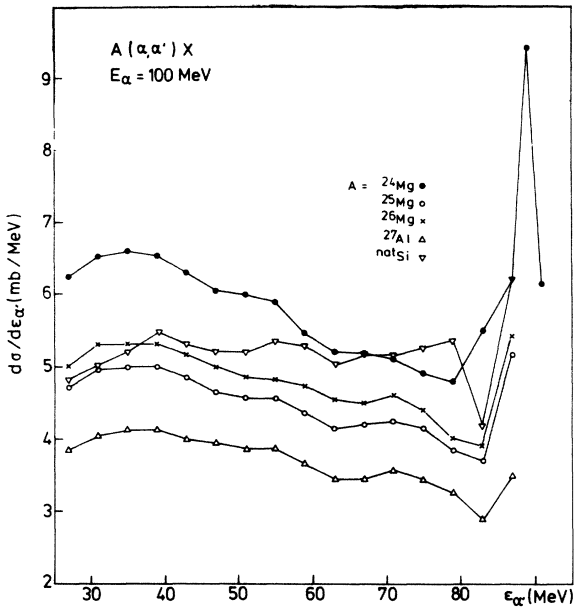

FIG. 3. Angle integrated cross sections for (α,α') reactions.

^{26}Mg coincide and for the odd-even nucleus ^{27}Al the smallest cross section has been measured. Another example is given in Fig. 3 for (α,α') reactions. The order is the same as for the (α,p) reactions except that the cross section for the even-odd nucleus ^{25}Mg is now smaller than for ^{26}Mg. Obviously, the reactions are favored for even-even nuclei especially when the target nucleus possesses an "α substructure." For the (α,α') reaction this result may

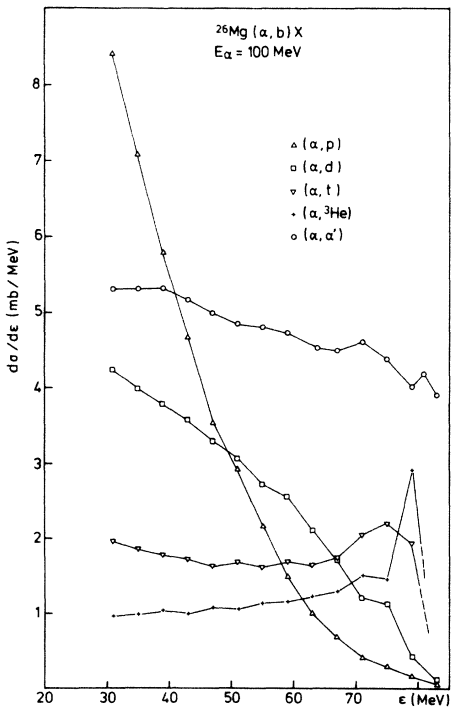

FIG. 4. Angle integrated cross sections for charged particles emerging from α plus ^{26}Mg reactions.

TABLE II. Comparison of the energy-differential cross sections for the (α,p) and (α,α′) reactions.

Target	^{24}Mg	^{25}Mg	^{26}Mg	^{27}Al	^{28}Si
			$\epsilon=45$ MeV		
$\frac{d\sigma(\alpha,p)}{d\epsilon}$ (mb/MeV)	5.58	4.10	4.14	3.68	4.86
$\frac{d\sigma(\alpha,\alpha')}{d\epsilon}$ (mb/MeV)	6.23	4.79	5.12	3.96	5.25
$\frac{d\sigma(\alpha,p)}{d\sigma(\alpha,\alpha')}$	0.90	0.86	0.81	0.92	0.93
			$\epsilon=65$ MeV		
$\frac{d\sigma(\alpha,p)}{d\epsilon}$ (mb/MeV)	1.18	0.832	0.80	0.793	1.04
$\frac{d\sigma(\alpha,\alpha')}{d\epsilon}$ (mb/MeV)	5.17	4.18	4.49	3.42	5.00
$\frac{d\sigma(\alpha,p)}{d\sigma(\alpha,\alpha')}$	0.23	0.20	0.18	0.23	0.21

be understood by assuming knockout contributions which are expected to be larger for ^{24}Mg and ^{28}Si than for the other target nuclei. However, recent $(\alpha,2\alpha)$ measurements on ^{58}Ni at $E_\alpha=140$ MeV have shown that knockout is a rather unlikely process when compared to other nonevaporative processes.[15] This finding is supported by the following. In Table II we compare the ratios $d\sigma(\alpha,\mathrm{p})/d\sigma(\alpha,\alpha')$ for two different ejectile energies. Surprisingly, these ratios are rather similar for the same ejectile energy. If the "α substructure" would increase the (α,α') yields, then the ratio would be smallest for ^{24}Mg and ^{28}Si. However, the opposite is true. Similar comparisons for the other composite ejectiles lead to the same results. From these observations we may conclude that composite particle emission does not strongly—if at all—depend on the individual structure of the target nucleus, at least for the nuclei in the present mass range.

In Fig. 4 we compare charged particle spectra from $^{26}\mathrm{Mg}+\alpha$ interactions with each other. The proton emission is the strongest channel for small energies. Whereas the proton spectrum has the steepest slope, the (α,α') channel has the flattest one. It is the strongest channel for energies above 50 MeV. The deuteron spectrum is in between with respect to shape and height. The t and ^{3}He spectra are very similar in shape. The latter is the weakest channel.

IV. COMPARISONS WITH MODEL CALCULATIONS

If we think of the continuous part of the proton spectra to be produced in a one step process, we can express the corresponding cross section in terms of the DWBA as

$$\frac{d\sigma}{d\Omega}=\frac{k_\mathrm{p}}{k_\alpha}\,|\,V_{fi}\,|^2\rho_f(U)dU\ , \tag{1}$$

with k denoting the momenta of the incident and outgoing particle, $|\,V_{fi}\,|$ an average matrix element, and ρ_f the density of final states in an excitation energy bin around U. Let us consider first the case of ^{27}Al. As has been pointed out by Griffin,[16] such a case is favored for the (α,p) reaction because ^{27}Al has an unpaired proton. In this case the matrix element should be large because the incident state wave function $\psi_i=\phi_\alpha\chi_T$ and the final state wave function $\psi_f=\phi_\mathrm{p}\chi_\mathrm{res}$ have large overlap due to the underlying structure: this may be expressed by the excitation of three protons and two neutrons in both states with respect to the core. On the other hand, for cases with paired protons a proton hole has to be excited additionally with respect to the core. Therefore, in these cases the matrix element should be small. The experimental finding, however, is the smallest cross section for ^{27}Al. This can be understood by further inspection of Eq. (1). The cross section depends also on the available phase space expressed in terms of the level density. Let us assume an Ericson type of level density, i.e.,

$$\rho_f(U)=\rho(p,h,U)=\frac{g^{p+h}U^{p+h-1}}{p!h!(p+h-1)!}\ , \tag{2}$$

with p and h being the number of excited particles and holes and g the single particle state density. As discussed above, an unpaired proton yields a three protons plus two neutrons equals $5p$ state. For a nucleus with only paired protons the result was three protons plus two neutrons plus one proton hole equals $5p+1h$ state. The second case has a much larger level density than the first one. If the level density is the dominating factor in Eq. (1), it is well understood why the most favorable nucleus by structure yields to the smallest (α,p) cross section.

The continuous cross sections are believed to come from multistep processes taking place in the continuum. Since different models have been recently reviewed,[17] we will give here a short description of the exciton coalescence model[18] only and then analyze the data in terms of it.

A. The exciton coalescence model

In terms of the exciton coalescence model (ECM) the reaction is thought to proceed from an initial state, as discussed above, through more complicated states until com-

plete statistical equilibrium is reached. The intermediate states are characterized by the number n of excited particles and holes commonly called excitons. Transitions between different states are assumed to occur only by two-body interactions. Therefore the complexity of states can only differ by $\Delta n = \pm 2$ or 0. In every state there is a certain probability for particles to be emitted. The relaxation process is calculated with the help of master equations.[17] The spreading rate $\lambda^{\downarrow}(n,E)$ may be calculated from nucleon-nucleon scattering in nuclear matter yielding[19]

$$\lambda^{\downarrow}(n,E) \sim \text{const} E \ . \tag{3}$$

The decay rate $\lambda^{\uparrow}$ is calculated from the principle of detailed balance. If we assume the level densities g_c of the composite system and g_R of the residual system to be equal, the decay rate is given by

$$\lambda^{\uparrow}(n,E) = \lambda^{\uparrow}(E) \frac{\mathrm{p}}{\mathrm{n}} \left[\left[1 - \frac{V_C + B_{\mathrm{p}}}{E} \right]^n + \left[1 - \frac{B_{\mathrm{n}}}{E} \right]^n \right] \tag{4}$$

with B denoting the binding energies and V_C denoting the Coulomb barrier. In the derivation of Eq. (4) a time reversed cross section of the form

$$\sigma_{\mathrm{inv}}(\epsilon) = \pi R^2 (1 - V_C/\epsilon) \tag{5}$$

is assumed and only neutron and proton emission considered. In Eq. (5) ϵ denotes the channel energy. The nucleon emission rate $\lambda^{\uparrow}(E)$ is given as

$$\lambda^{\uparrow}(E) = \frac{2s+1}{\pi^2 \hbar^3} E \mu \sigma_{\mathrm{inv}}(E) \frac{1}{g} \tag{6}$$

with s the spin degeneracy and μ the reduced mass.

Composite particles may be formed during such an equilibration process when excited nucleons have proper spin and isospin and when their momenta are confined within a sphere having radius P_0 around the momentum P_c of a leading nucleon. The cross section is then given by an incoherent sum over contributions from states having different exciton numbers[17]

$$\frac{d^2\sigma}{d\epsilon d\Omega} = \sum_{\substack{n=n_0 \\ \Delta n = 2}}^{\bar{n}} f(n,x) W_x(\epsilon,E) A(n - p_x + p_y, \Omega) \times \theta(n - p_x + p_y) \int_0^{t_{\mathrm{eq}}} P(n,t) dt \ . \tag{7}$$

The first quantity is a correction for using only one Fermi gas for nucleons instead of different ones for protons and neutrons. W_x is given by

$$W_x(\epsilon,E) = \frac{2s_x + 1}{\pi^2 \hbar^3} \epsilon \mu \sigma_{\mathrm{inv}}(\epsilon) p \tilde{F} \left[\tfrac{4}{3} \pi (P_0/uc)^3 \right]^{p_x - 1} \tag{8}$$

with u and c denoting the nucleon mass and vacuum velocity of light, and with $\tilde{F}$ the probability density to have the right sharing of energy between the ejectile and the residual system.[17] $\tilde{F}$ contains mainly level densities

$$\tilde{F} = \binom{p}{p_x}^{-1} \frac{\rho(p - p_x, h, E - \epsilon - B_x)}{\rho(p,h,E)} \frac{\rho(p_x, v, \epsilon)}{g} \ . \tag{9}$$

If we assume a level density of the type Eq. (2), the same single-particle level density, and neglect the binding energy, the relation

$$\int_0^E \tilde{F} \, d\epsilon = 1 \tag{10}$$

holds. The number of particles in the projectile is denoted by p_y and by p_x that in the ejectile. In Eq. (7) A is a function containing angle information only and $P(n,t)$ is the occupation probability of a state with n excitons at time t measured in terms of the absorption cross section.

B. Data analysis in the framework of the exciton coalescence model

1. Proton emission

As already discussed in the preceding subsection the initial degree of freedom is a crucial model parameter. From a naive point of view one might assume that in the first projectile-target interaction the complex projectile dissolves into its constituents by simultaneous excitation of one particle and one hole in the target nucleus. Such an initial exciton number $n_0 = p_y + 1p + 1h$ has been widely used in the analysis of data.[3,20] However, this number, for the present case $n_0 = 6$, is not in agreement with the number $n_0 = 5$ for the case having an unbound proton as has been discussed above. Recently, this intuitive picture has been given up leading to an energy dependence of n_0.[21] As a starting point of the analysis we have performed model calculations employing n_0 equals five particles plus one hole. In the calculations, furthermore, the single particle state density g was assumed to be the same for all systems, namely to the one with the primary composite nucleus. This quantity was allowed to vary as to fit the data. To make the effect of the fit more clear we assume

$$g_c = \frac{A}{13.3 \text{ MeV}} f \ , \tag{11}$$

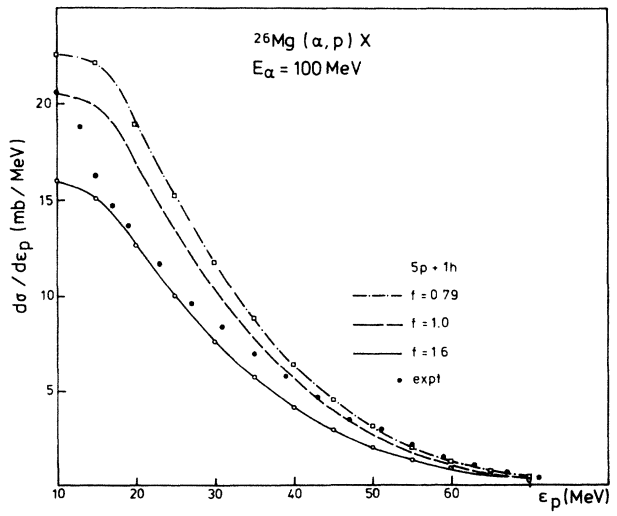

FIG. 5. Comparison between energy differential cross sections and ECM calculations with $n_0 = 5p + 1h$. The level density was scaled by factors f indicated in the figure [see Eq. (11)].

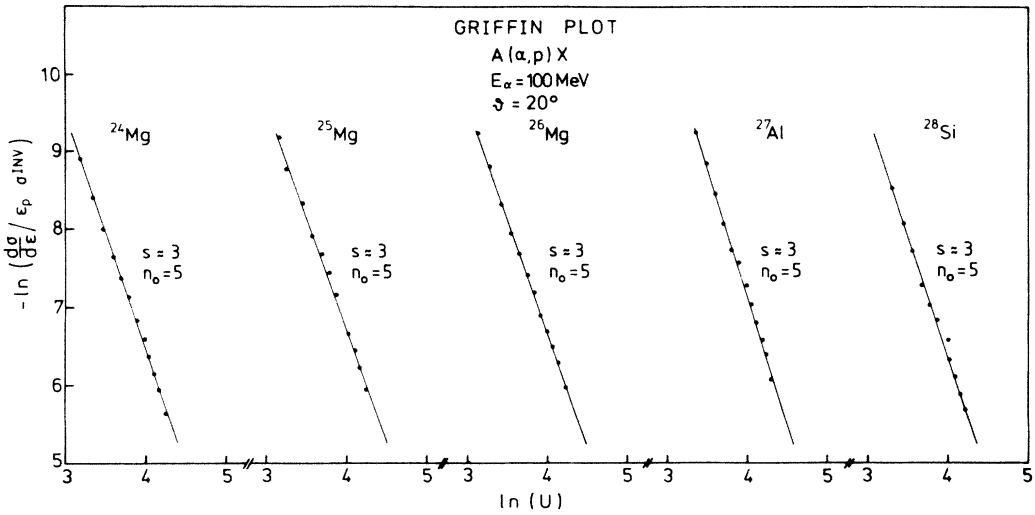

FIG. 6. Griffin-plot analysis of proton spectra.

with f a measure for the deviation from the average single particle state density corresponding to a level density parameter ($a=g\pi^2/6=A/8$ MeV). On a *semilogarithmic* scale we obtain a good reproduction of the data. The influence of f seems to be rather small. This situation, however, changes drastically when we make the comparison on a *linear* scale which is shown in Fig. 5 for the case of ^{26}Mg as target nucleus. The low energy part is best reproduced by a value $f=1.6$, while the high energy part favors $f=0.79$ more. Obviously, it is not possible to reproduce the data on a *linear* scale with only one value for f. We then have determined n_0 from the data itself by means of a Griffin plot analysis.[17] One can assume that the term depending on n_0 in Eq. (7) is the dominant one. This is a good approximation for large energies ϵ of the emerging proton or, in other words, small residual excitation energy $U=E-B_p-\epsilon$, and for small detection angles. In this approximation the cross section is given by

$$\frac{d^2\sigma(\epsilon,\vartheta)}{d\epsilon\, d\Omega} \propto \epsilon\sigma_{\rm inv}(\epsilon)U^{p_0+h_0-2} ,$$

which can be easily transformed into the equation of a straight line

$$\ln\left[\frac{1}{\epsilon\sigma_{\rm inv}(\epsilon)}\frac{d^2\sigma(\epsilon,\vartheta)}{d\epsilon\, d\Omega}\right]=(p_0+h_0-2)\ln U+\text{const} . \tag{12}$$

A corresponding plot of the data is named after Griffin. We have made such plots for our data taken at 20° which are shown in Fig. 6. Fits of straight lines to the data points yield slope parameters s of approximately three and therefore $n_0=p_0+h_0=5$. Unfortunately, this type of analysis does not show the partition of excitons with particles and holes. To answer the question which is the right choice we have performed model calculations employing n_0 equals four particles plus one hole and n_0 equals five particles plus zero hole, keeping the particle number close to the number of nucleons in the projectile. The results of such calculations are shown in Figs. 7 and 8 again for the data from the ^{26}Mg target. As in the calculations discussed above, the single-particle state density

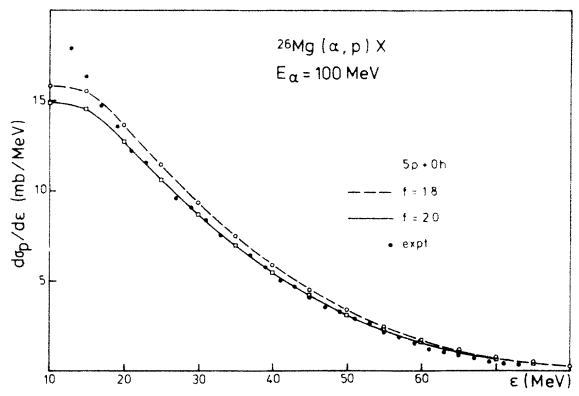

FIG. 7. Comparison between data for ^{26}Mg target nuclei and ECM calculations employing $n_0=5p+0h$ and f values as indicated in the figure.

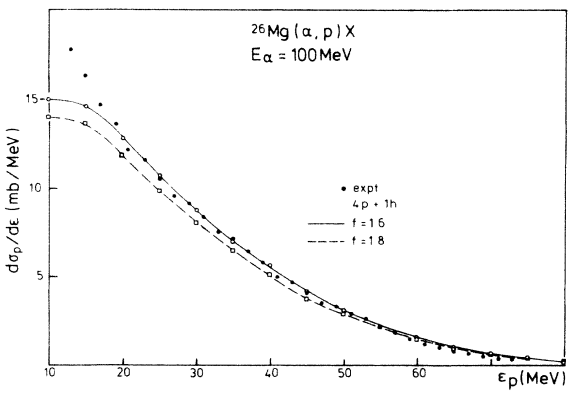

FIG. 8. Same as Fig. 7, but for $n_0=4p+1h$.

TABLE III. Scaling factors f for the single particle state density [Eq. (11)].

Composite nucleus	^{28}Si	^{29}Si	^{30}Si	^{31}P	^{32}S
Structure	even-even	even-odd	even-even	even-odd	even-even
f	1.4	1.8	1.6	3.2	1.8

was adjusted to fit the data. For both calculations we obtain excellent agreement on a *linear* scale. The value f, which for $n_0=6$ was approximately 1, increases to 1.6 and 2.0, respectively. For the cases of the other target nuclei only the choice n_0 equals four particles plus one hole yielded satisfactory results. We have therefore continued the analysis with this number. The deduced f values are shown in Table III. First we see a linear increase in f for the even-even nuclei. Surprisingly, the "α-particle" nuclei ^{28}Si and ^{32}S do not show a strong deviation from the average. For ^{31}P, which has an unbound proton, a rather large single particle state density is obtained. This means that also the total level density is large in contrast to what should be expected from the discussion above. We will come back to this point later. The sensitivity of the analysis can be estimated from the comparison of two calculations with data for the case of ^{27}Al as target and is shown in Fig. 9. One calculation is for $f=1.8$ which is close to the average value. This calculation overestimates the data over the whole energy range and expresses the need for a larger single particle state density as employed in the second calculation shown. Another important ingredient in the calculations which strongly influences spectral heights and spectral shapes is the secondary chance emission, i.e., emission of protons from daughter nuclei. In Fig. 10 the contributions from the composite system (first chance emission) and from daughter nuclei produced via proton emission and neutron emission are separately shown together with their sum and data for the case of ^{25}Mg target nuclei. The method of how to do such calculations is discussed in Ref. 17. To summarize the results of the analysis we can state that n_0 equals four particles plus one hole is the preferable choice for the initial exciton number and that data are reproduced even on a linear scale by adjustment of one quantity, namely the single particle state density.

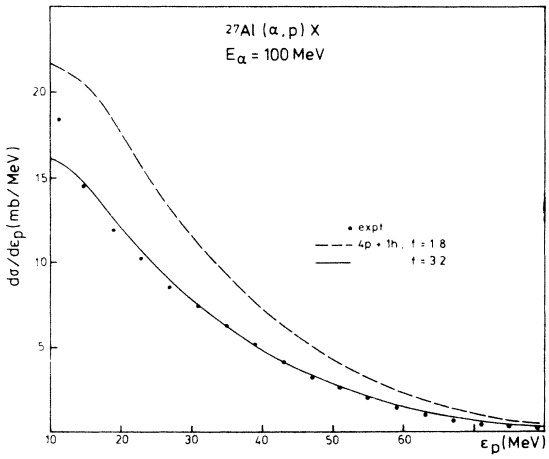

FIG. 9. Same as Fig. 8, but for ^{27}Al target nuclei.

2. *Complex particle emission*

For the analysis of complex particle spectra one has one more model parameter: the coalescence radius P_0. This radius was obtained by adjusting

$$\gamma_x=[\tfrac{4}{3}\pi(P_0/uc)^3]^{P_x-1} \tag{13}$$

to fit the data [see Eq. (8)]. As already mentioned in the discussion of the data, there is contamination to the pure preequilibrium continuum from other reaction mechanisms. In the case of proton emission they represent only a small fraction of the cross section. However, the situation is different for other particles in the exit channel. We have therefore fitted the model calculations to the data for only those energy regions where the cross sections are more or less free from contamination. A typical result is shown in Fig. 11 for complex particle emission from the ^{25}Mg + α system. The spectral shapes are well reproduced. With increasing mass number of the emitted particle the spectra become less steep. This feature is nicely reproduced by the calculations. We would like to stress once more the point that the comparison is made on a linear scale. The deduced coalescence radii P_0 for the different particles emerging from the different composite systems are listed in Table IV. They are rather uniform and do not seem to depend on the individual target nucleus; although, the latter have a different and individual structure as seen in the discussion of the proton emission. This indicates that the mechanism responsible for the for-

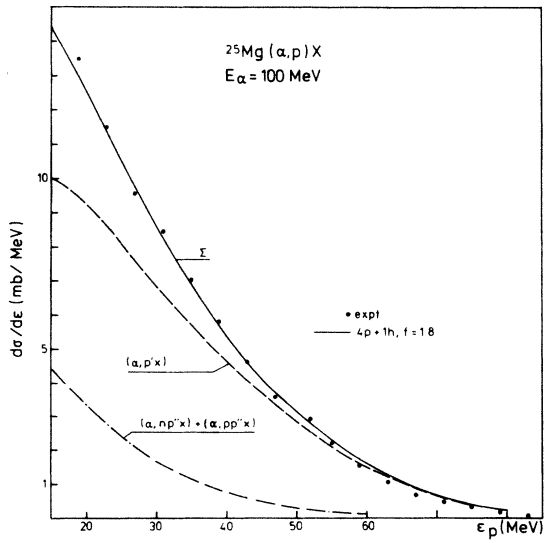

FIG. 10. Same as Fig. 8, but for ^{25}Mg target nuclei. The contributions from the composite system as well as from daughter nuclei produced by neutron or proton emission are also shown.

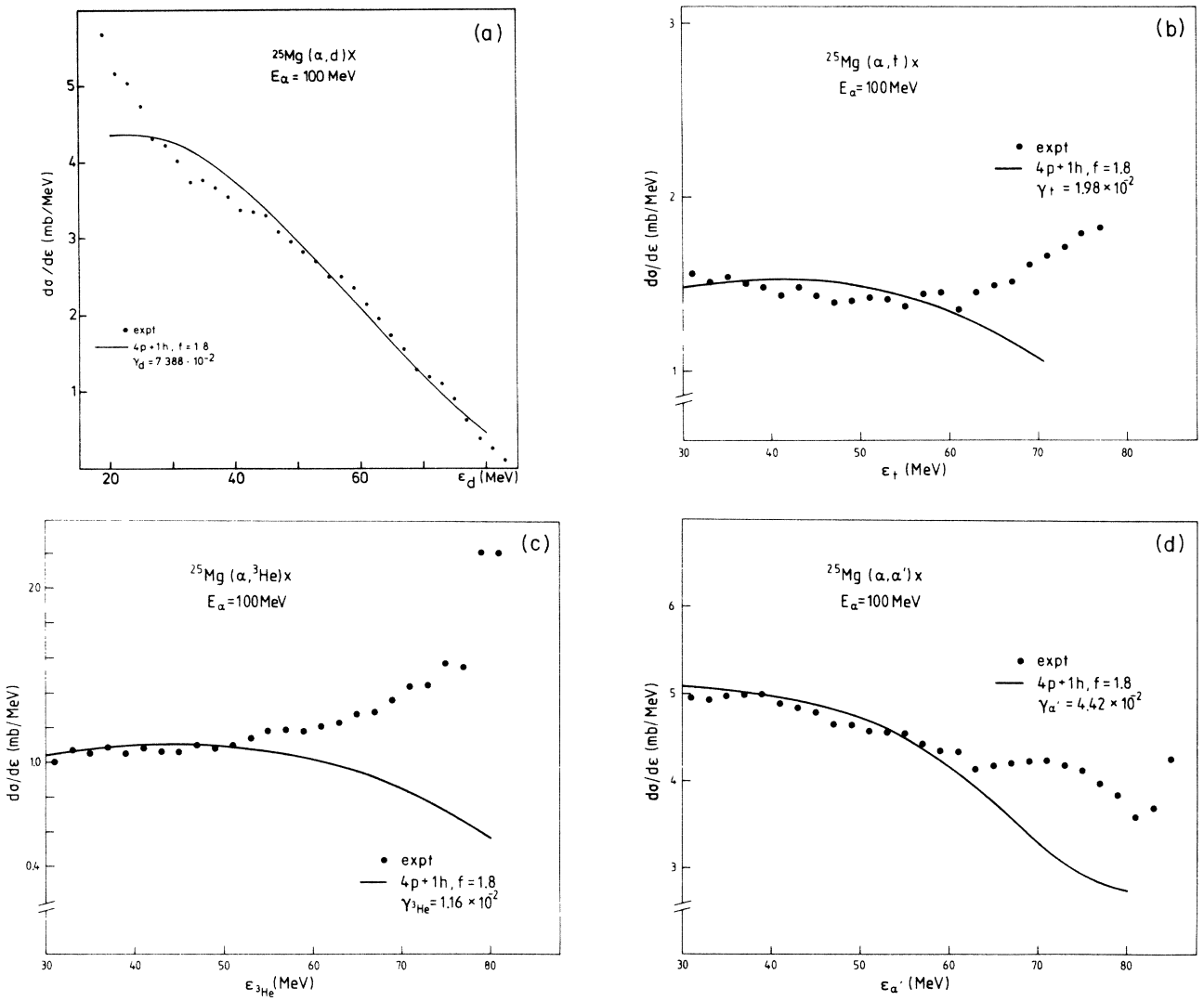

FIG. 11. Angle integrated cross sections for the indicated reactions are compared with ECM calculations. Spectra for d, t, ^{3}He, and α-particle emission are shown in parts (a), (b), (c), and (d), respectively.

mation of the complex particles does not strongly depend on the target nucleus as is the case for transfer reactions to bound states. Also in the study of the excitation functions for inclusive t production, a very weak A dependence of the triton formation probability was observed.[22] For α-induced reactions a value $P_0=298$ MeV/c is obtained for targets spanning the periodic table from aluminum to gold. This value may be compared with the mean for t production from the present investigation which is $P_0=300.6$ MeV/c. All mean values are shown in Table V together with coalescence radii $\tilde{P}_0$ from which spin alignment and phase factors are explicitly removed according to[23]

$$(\tilde{P}_0^3)^{N+Z-1}=(P_0^3)^{N+Z-1}\frac{2^{N+Z}}{(N+Z)^3(2s+1)} \tag{14}$$

TABLE IV. Deduced coalescence radii P_0 (MeV/c) for the different exit channels.

Composite nucleus	P_0 (MeV/c) d	t	^{3}He	α
^{28}Si	263.3	299.3	284.2	405.2
^{29}Si	244.4	303.0	277.1	412.0
^{30}Si	252.3	302.4	275.5	407.2
^{31}P	254.2	301.2	289.0	405.2
^{32}S	256.1	297.1	302.2	403.7

TABLE V. Coalescence radii and reduced coalescence radii for the mean values of Table IV. The radii in coordinate space are from a phase space relation [R, Eq. (15)], or from Eqs. 16 and 17 (R_x) assuming a Gaussian distribution. Root-mean-square radii R_m are also shown for comparison.

x=particle type	P_0 (MeV/c)	$\tilde{P}_0$ (MeV/c)	R[a] (fm)	ν_x (fm^{-2})	R_x (fm)	R_m[b] (fm)
d	254.1	139.8	3.41	0.415	1.90	2.095
t	300.6	218.7	2.18	0.698	1.47	1.70
^{3}He	285.6	207.7	2.30	0.629	1.54	1.87
α	406.7	348.6	1.37	1.50	1.00	1.63

[a]Obtained from the phase space relation Eq. (15).
[b]From Ref. 25.

with N and Z the neutron and proton number of the emerging particle and s its spin as before. From these values radii R in coordinate space can be evaluated if we only assume the phase space relation to be valid

$$R=\left[\frac{3}{4\pi}\right]^{2/3}\frac{2\pi\hbar}{\tilde{P}_0}\ . \tag{15}$$

These values are also shown in Table V. As in relativistic nucleus-nucleus collisions we observe a decrease of the radii with increasing mass number of the emitted composite.[23] Mekjian concluded from this behavior that R represents the volume from which particles are being emitted and that α particles are emitted in an earlier stage than t and ^{3}He which are from an earlier phase than deuterons. On the other hand it was shown in Ref. 20 that the radii deduced from experiments with the help of the phase space relation Eq. (15) are close to the radii of the free clusters. From this finding an alternative interpretation emerges: when nucleons are confined within the phase space of the corresponding light nucleus they are emitted as such. In contrast to the model raised by Mekjian,[23] no equilibrium is necessary for cluster formation. More recently, Sato and Yasaki[24] have also given up the picture of achieved equilibrium in the volume $\frac{4}{3}\pi R^3$. They calculated coordinate space radii in the framework of the density matrix formalism. If we apply their final results to the present data we obtain negative values for the range parameters ν of the reaction volume assumed to have Gaussian shape in the cases of d and α emission. We take this as an additional hint against the interpretation of the coordinate space volume as reaction volume. One can apply the formalism of Ref. 24 without distinguishing between the cluster x with range parameter ν_x and the reaction volume yielding to[17]

$$\left(\tfrac{1}{2}\right)^{N+Z-2}\left(\tfrac{4}{3}\pi\tilde{P}_0^{\,3}\right)^{N+Z-1}=(2\pi\nu_x)^{3/2(N+Z-1)}(Z+N)^{-3/2}\ . \tag{16}$$

From this relation we obtain the range parameters ν_x given also in Table V for the present mean radii $\tilde{P}_0$. From ν_x the root mean square radii R_x are evaluated according to

$$R_x=\sqrt{3/(2\nu_x)}\ . \tag{17}$$

These values are also shown in Table V together with root-mean-square charge radii for the free clusters R_m taken from literature.[25] Both ways of deriving radii, i.e., Eq. (15) and Eqs. (16) and (17) yield values close to those for the free clusters. In all cases the sharp cutoff values R are larger than the root mean square radii R_x. The latter are somewhat smaller than the root mean square radii for the free clusters, except for deuterons.

3. *Angular distributions*

Besides angle-integrated yields the exciton coalescence model is also able to predict angular distributions.[18,20] The corresponding quantity $A(n,\Omega)$ in Eq. (7) is the probability that in a n-exciton state there is a fast nucleon with direction $\Omega=(\vartheta,\phi)$. Because we are not dealing with polarized particles A is independent of the azimuth ϕ. The θ or step function in Eq. (7) makes sure that there is at least one recoiling nucleon.[20] Calculations have been performed with two different choices for the initial distribution probability. One choice is[26]

$$A(n_0,\Omega)=\alpha\cos(\beta\vartheta)\theta(\pi/2-\beta\vartheta) \tag{18}$$

with $\beta=k_\alpha R/8$, which takes into account that only a limited angular momentum can be transferred to the composite system. The other choice takes into account the exponential slopes observed in the data[27]

$$A(n_0,\Omega)=a\exp(-b\vartheta) \tag{19}$$

with $b\sim 8$/rad. The overall normalization constants α and a are obtained from the relation

$$\int A(n_0,\Omega)d\Omega=1\ . \tag{20}$$

Results of such calculations for the ^{24}Mg(α,p)x reactions are shown in Fig. 12. The model calculations are close to the data for angles smaller than 60°. The calculation with the exponential dependence Eq. (19) reproduces the data in this interval better than the one with Eq. (18). For angles larger than 60° there is a large discrepancy for both types of calculations. This failure is observed for all reactions measured. The same overestimation for backward angles as ECM does hold for the empirical estimate according to Kalbach and Mann.[28] In this framework the cross section is given by

$$\frac{d^2\sigma(\epsilon,\vartheta)}{d\epsilon\,d\Omega}=a_0\sum_{e=0}^{l_{\max}}b_e(\epsilon)P_l(\cos\vartheta) \tag{21}$$

with the reduced coefficients b_e obtained from a parametrization of experimental data.[28] The calculations made include partial waves up to $l_{\max}=20$. The factor a_0 is

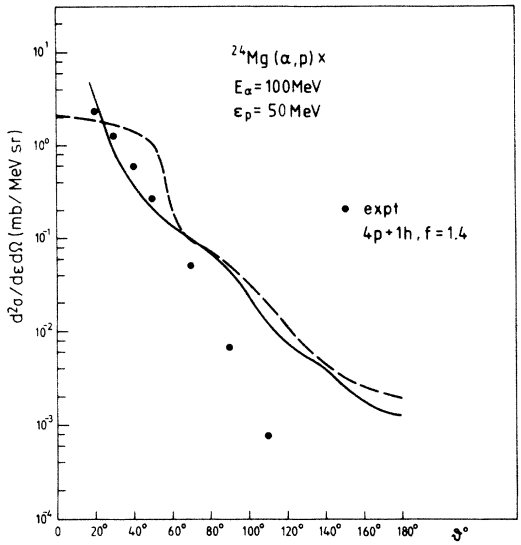

FIG. 12. Angular distribution for the indicated reaction. Calculations employing an initial angular distribution function Eq. (18) are shown as a dashed curve; those employing Eq. (19) are shown as a solid curve.

given by the condition that the integral over the unit sphere of Eq. (21) yields the experimental angle-integrated cross section. One comparison with data is shown in Fig. 13. Both calculations, ECM and the one according to Ref. 28, give very similar results. The failure of the parametrization method is surprising because it worked rather satisfactory for large angles and moderate ejectile energies.[17] In order to investigate this unexpected angular behavior of the present data we have compared angular distributions with those obtained from 90 MeV α particle induced reactions on ^{54}Fe (Ref. 27). In Fig. 14 the angular distributions

$$\frac{d^2\sigma(\epsilon,\vartheta)}{d\epsilon\, d\Omega} \Big/ \frac{d\sigma(\epsilon)}{d\epsilon} = \frac{d^2\sigma(\epsilon,\vartheta)}{d\sigma(\epsilon) d\Omega}$$

are shown for $(\alpha,{}^3\mathrm{He})$ and (α,α') reactions on ^{25}Mg and ^{54}Fe. In the case of ^{3}He emission the ejectile energy is 68 MeV which corresponds to a region in the breakup bump. The data agree with each other for small angles, i.e., smaller than 60°. For larger angles the data for the lighter target nucleus seem to fall off more steeply than those for ^{54}Fe. The prediction of Eq. (21), which is the same for both reactions, again overestimates the yields of the $^{25}\mathrm{Mg}+\alpha$ reactions for large angles by two orders of magnitude. The same deviation between reactions on the light nuclei and ^{54}Fe holds also for energy intervals completely dominated by pure preequilibrium (see Fig. 12). The angular distributions for the $^{54}\mathrm{Fe}(\alpha,\alpha')$ case are reproduced by Eq. (21). From this analysis we can conclude that the angular distributions depend on the target mass at least for large angles. Such a dependence is not accounted for by ECM and is in contrast to the findings of Ref. 28.

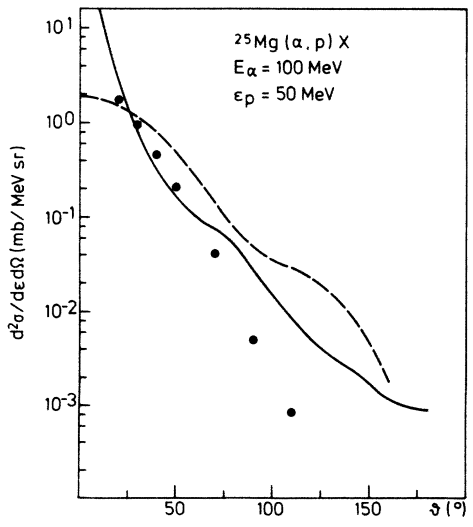

FIG. 13. Angular distribution for the indicated reaction. The ECM calculation is shown as a solid curve and the parametrization (Ref. 28) is normalized to the experimental angle integral as a dashed curve.

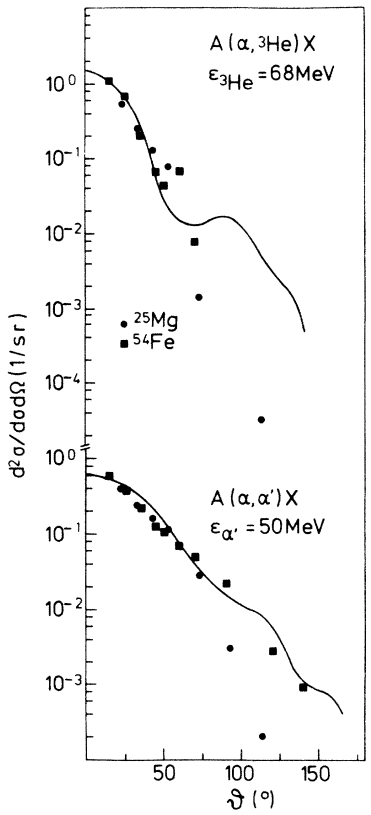

FIG. 14. Angular distributions normalized to 1 for $(\alpha,{}^3\mathrm{He})$ and (α,α') reactions. The data from ^{25}Mg are shown as dots, data from ^{54}Fe as squares. The parametrization from Ref. 28 is shown as curves.

V. DISCUSSION

As already mentioned above, the proton data infer an initial exciton number $n_0=5$. From model calculations the preferable choice was found to be $n_0=4p+1h$ in-

dependent of the structure of the target nuclei. This is surprising because ^{27}Al has an unpaired proton which could be more easily removed in an (α,p) reaction than a paired proton which is the case for the other target nuclei studied. The expected difference in n_0 as expected from nuclear structure—see the discussion around Eq. (1)—is not observed. This can be taken as evidence that not only the weakest bound nucleon participates in the reaction. From plane wave calculations for ^{27}Al(p,p') and (p,n) reactions at 90 MeV bombarding energy it was found[29] that 60% of the nucleons from the outermost shell and 20% from the inner shell participate in the reaction which yields approximately ten nucleons for ^{27}Al.

The differences in the absolute heights for the charged particle spectra yielding always largest cross sections for ^{24}Mg and smallest for ^{27}Al, may be due to differences in the absorption cross sections. For the ECM calculations these were calculated according to

$$\sigma_{\text{abs}}=\pi r_0^2(A_T^{2/3}+A_p^{2/3})(1-V_C/E_{\text{p}}) . \tag{22}$$

To check such a possibility we have calculated σ_{abs} from optical model parameters for 104 MeV α particles on ^{24,26}Mg and ^{28}Si (Ref. 30). In these calculations no such deviations were observed which are large enough to explain the present data with $f=1$ in Eq. (11). The same is true if we do not apply a constant r_0 in Eq. (22), but charge density radii obtained from electron scattering.[25] Such values yield only a 10% reduction in the absorption cross section for ^{27}Al when compared to ^{24}Mg, whereas a factor of approximately 1.5 is needed to reproduce the experimental findings.

The large values for f deduced from the present data may be due to model approximations and thus do not reflect the underlying physics but the shortcomings of the model. One approximation that was made assumed the same single particle state density for the composite as well as for the residual system. Such a prescription is motivated by the following. For nucleon emission one can formally derive Eq. (8) by applying the principle of detailed balance. Then the corresponding state densities in Eq. (9) contain g_R and g_c, the single particle state densities of the residual and the composite system, respectively. Then even small differences in g_R and g_c can result in large f values because we have

$$\frac{1}{f}=\left[\frac{g_R}{g_c}\right]^{n-1} . \tag{23}$$

If we assume that the term depending on n_0 is the dominating one, we have already an exponent 4 for the present case. It should be mentioned that Akkermans *et al.* (Ref. 31) have analyzed the (n,n') data of Ref. 6 within a slightly different exciton model formulation. They have adjusted g_R and have kept g_c fixed to $A/13$ MeV. Their adjusted values differ up to a factor of 2 from this mean value for nuclei in the region of interest. Instead of adjusting the single particle state density one could account for odd-even effects by introducing an energy shift, as done for low energy (p,n) reactions.[32] A pairing shift of $2\Delta\sim 4$ MeV for the ^{30}Si nucleus reached in the ^{27}Al(α,p) reaction would have a large effect on the level density and, therefore, on the corresponding cross section. We will not, however, go into a detailed discussion of the forward shifted or the backward shifted Fermi gas models. Although there is a large discrepancy between forward and backward shifted level-density formulae, both descriptions are applied in statistical model calculations and it seems highly desirable to study the problem in the context of preequilibrium reactions. However, such an investigation is beyond the scope of the present work. Another shortcoming of the present model may be the assumption of equally spaced single-particle states. The Fermi gas model predicts $g\sim\epsilon^{1/2}$. However, the approximation made is the same for all target nuclei studied. A possible break down of the validity of this assumption can not explain the differences observed. It is furthermore well known that the Fermi gas estimate accounts for only one-half of the empirical value $g(\epsilon_F)=A/13$ MeV. This discrepancy cannot be removed by additional treating of surface and curvature corrections.[33] We may conclude this discussion by stating that we have observed differences in the single particle state densities at least on a relative basis. On the other hand we may look at Eq. (8) with the following interpretation. We can rewrite Eq. (8) as

$$W_x(\epsilon,E)=\lambda_x^{\uparrow}(\epsilon)g_x p\tilde{F}\gamma_x . \tag{24}$$

Then $\tilde{F}$ is the probability density to have the n-exciton system in a state where in the residual system n-p_x excitons share the excitation energy U while p_x excitons share the energy E-U. The factor γ_x contains the spectroscopic information whether a composite subsystem is really formed or not and g_x is its single-particle state density. Particles are emitted from the system at a rate $\lambda_x^{\uparrow}$ which is calculated from detailed balance as in Ref. 34. In such an interpretation which has some similarity to the hybrid model,[35] $\tilde{F}$ contains only one particle state density, namely g_c. Our data are suited to distinguish between both points of view. If the first interpretation is valid then we should get the same type of individual adjustment not only for proton emission but also for other composite particle emission. If so, the influence of different level densities must be contained in γ_x or the corresponding coalescence radii P_0. However, these values do not show such an odd-even effect as f does. The γ_x values are constant within 20%. From this finding we conclude that the second point of viewing the process is the right one.

Furthermore, the complex-particle emission is independent from the structure of the target nucleus. This finding supports the assumption of coalescence amongst nucleons participating in the reaction. Significant contributions from knockout of preformed particles can therefore be excluded. The exciton coalescence model is able to reproduce angle integrated data on a *linear* scale. In most analyses published so far comparisons between data and model calculations were done on a semilogarithmic scale. The model fails to reproduce large angle yields. The same is true for the parametrization of Ref. 28. The present data have a steeper slope with respect to the angle than those for heavy nuclei.

[1]F. E. Bertrand and R. W. Peelle, Phys. Rev. C **8**, 1945 (1973).
[2]F. E. Bertrand, R. W. Peelle, and C. Kalbach-Cline, Phys. Rev. C **10**, 1028 (1974).
[3]J. R. Wu, C. C. Chang, and H. D. Holmgren, Phys. Rev. C **19**, 659 (1979); **19**, 370 (1979); **19**, 698 (1979).
[4]U. Bechstedt, H. Machner, G. Baur, R. Shyam, C. Alderliesten, O. Rousshid, A. Djaloeis, P. Jahn, C. Mayer-Böricke, F. Rösel, and D. Trautmann, Nucl. Phys. **A343**, 221 (1980).
[5]O. Bousshid, H. Machner, C. Alderliesten, U. Bechstedt, A. Djaloeis, P. Jahn, and C. Mayer-Böricke, Phys. Rev. Lett. **45**, 980 (1980).
[6]D. Hermsdorf *et al.*, Zentralinstitut für Kernforschung, Rossendorf bei Dresden, Report Zfk-277, 1974.
[7]C. M. Castaneda, J. L. Ullmann, F. P. Brady, N. S. P. King, and M. Blann, Phys. Rev. C **28**, 1439 (1983).
[8]M. Blann, L. F. Hansen, T. Komoto, B. A. Pohl, C. Wong, S. M. Grimes, Y. Holler, W. Scobel, and M. Trabandt, in *Proceedings of the Workshop on Coincident Particle Emission from Continuum States in Nuclei, Bad Honnef, 1984,* edited by H. Machner and P. Jahn (World-Scientific, Singapore, 1984), p. 46.
[9]W. Scobel, M. Blann, T. T. Komoto, M. Trabandt, S. M. Grimes, L. F. Hansen, C. Wong, and B. A. Pohl, Phys. Rev. C **30**, 1480 (1984).
[10]M. Blann, S. M. Grimes, L. F. Hansen, T. T. Komoto, B. A. Pohl, W. Scobel, M. Trabandt, and C. Wong, Phys. Rev. C **32**, 411 (1985).
[11]G. Seniwongse, H. Machner, P. Jahn, M. Nolte, M. Rogge, and P. Turek, Institut für Kernphysik, Jülich, Report Jül-Spez-312, 1985.
[12]A. Budzanowski, G. Baur, C. Alderliesten, J. Bojowald, C. Mayer-Böricke, W. Oelert, and P. Turek, Phys. Rev. Lett. **41**, 635 (1978).
[13]J. R. Wu, C. C. Chang, and H. D. Holmgren, Phys. Rev. Lett. **40**, 1013 (1978).
[14]A. Kiss, C. Mayer-Böricke, M. Rogge, P. Turek, and S. Wiktor, Phys. Rev. Lett. **33**, 1188 (1976).
[15]H. Machner, U. Bechstedt, A. Budzanowski, P. Jahn, and C. Mayer-Böricke, Phys. Rev. C **33**, 91 (1986).
[16]J. Griffin, Phys. Lett. **24B**, 5 (1967).
[17]H. Machner, Phys. Rep. **127**, 309 (1985).
[18]H. Machner, Phys. Lett. **86B**, 129 (1979).
[19]H. Machner, in *Proceedings of the 17th Summer School on Nuclear Structure, Mikolajki, Poland, 1985,* edited by Z. Wilhelmi and M. Kicińska-Habior (Harwood, New York, in press).
[20]H. Machner, Phys. Rev. C **21**, 2695 (1980).
[21]H. Machner, Z. Phys. A **321**, 577 (1985).
[22]M. Merkel and H. Münzel, in Proceedings of the 3rd International Conference on Nuclear Reaction Mechanisms, Varenna, Italy, 1982, edited by E. Gadioli, Ric. Sci. Educ. Permanente, Suppl. **28**, 299 (1982).
[23]A. Mekjian, Phys. Rev. C **17**, 1051 (1978).
[24]H. Sato and K. Yasaki, Phys. Lett. **98B**, 153 (1981).
[25]C. W. de Jager, H. de Vries, and C. de Vries, At. Data Nucl. Data Tables **14**, 479 (1974).
[26]G. Mantzouranis, D. Agassi, and H. A. Weidenmüller, Z. Phys. A **276**, 145 (1976).
[27]H. Machner, U. Bechstedt, A. Djaloeis, and P. Jahn, Phys. Rev. C **26**, 411 (1982).
[28]C. Kalbach and F. M. Mann, Phys. Rev. C **23**, 112 (1981).
[29]A. M. Kalend, B. D. Anderson, A. R. Baldwin, R. Madey, J. W. Watson, C. C. Chang, H. D. Holmgren, R. W. Koontz, J. R. Wu, and H. Machner, Phys. Rev. C **28**, 105 (1983).
[30]H. Rebel, G. W. Schweimer, G. Schatz, J. Specht, R. Löhken, G. Hauser, D. Habs, and H. Klewe-Nebenius, Nucl. Phys. **A182**, 145 (1972).
[31]J. M. Akkermans, H. Gruppelaar, and G. Reffo, Phys. Rev. C **22**, 73 (1980).
[32]S. M. Grimes, J. D. Anderson, J. W. McClure, R. A. Pohl, and C. Wong, Phys. Rev. C **7**, 343 (1973); S. M. Grimes, J. D. Anderson, and C. Wong, *ibid.* **13**, 2224 (1976).
[33]G. Handloser and W. Stocker, Nucl. Phys. **A441**, 491 (1985).
[34]G. D. Harp and J. M. Miller, Phys. Rev. C **3**, 1847 (1971).
[35]M. Blann, Phys. Rev. Lett. **27**, 337 (1971).